The 2009 IEEE/RSJ International Conference on
Intelligent Robots and Systems
October 11-15, 2009 St. Louis, USA

Real Time Motion Generation and Control for Biped Robot -2nd Report: Running Gait Pattern Generation-

Toru Takenaka, Takashi Matsumoto, Takahide Yoshiike and Shinya Shirokura

Abstract—**Bipedal running can easily result in a fall due to poor availability of the ground reaction force at the boundary of the flight and support phases. We propose methods to decompose and synthesize a running gait pattern into vertical, horizontal and rotational components so that time-dependent ground friction limits are satisfied. We also extend previously proposed boundary condition, the divergent component of motion, for switching walking gait patterns into running which involves vertical acceleration of the center of gravity. Using these techniques, running at 10 km/h is achieved on a real robot whose dimension are same as ASIMO.**

I. Introduction

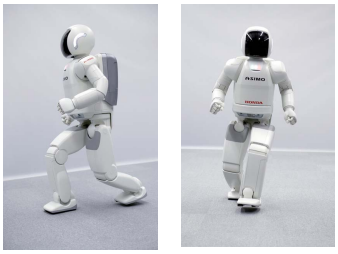

Fig. 1 Running biped robot system (ASIMO)

For biped robots [1][2] (Fig. 1) to exist around and collaborate with human, they need abilities to react quickly against unknown events including avoiding collision with previously unknown obstacles and maintaining balance under external disturbances by taking steps.

One kind of agility is ability to run. In this paper running for a biped robot is defined as a gait in which at some point in every cycle of the trajectory both feet are off the ground at the same time. Running has several advantages over walking including

1. When the robot is in the flight phases, the entire body of the robot is moving forward and can step longer beyond the kinematic constraint of leg.
2. Running involves larger ground reaction force in vertical direction compared to walking thus can generate larger ground reaction force in horizontal direction to realize faster motions.

Raibert [12] realized running with a linearly actuated robot by controlling the landing position. Nagasaki et al. [3] used similar methods.

Running gaits for biped robots include phases in which the ground reaction force equals to zero. Trajectories satisfying this property is to switch dynamics constraints at the boundary of flight and support phases (Nagasaka et al. [4], Tajima et al. [5], Kwon et al. [13]). In these approaches, the trajectory during the flight phases was designed so that the center of gravity (CoG) of the robot is in a free fall motion and its angular moment about the CoG is reserved. During the support phases, approaches similar to design of walking gait pattern using ZMP are employed to generate a trajectory [9]. Fujimoto et al. [10] solves different dynamics equations between the flight and support phases, and generates motion by minimizing energy.

Immediately before the foot leaves or after the foot lands, the available ground reaction force and moment are small. However, these approaches do not consider about this insufficiency of the ground reaction force and moment. This cause the horizontal component of the ground reaction force to reach the friction limit and the robot may fall down. In addition, these methods cannot be applied to jogging motion in which the CoG moves in vertical direction without flight phase.

We propose a method to decompose running motion of biped robots into translational and rotational components. The translational component is further devided into vertical and horizontal components, and the rotational component refers to rotation about the horizontal axis. Running gaits are designed by synthesizing these three motions while satisfying the ground reaction force limits. Our approach can generate gait patterns with large region of stability in real time to react to unexpected disturbances. We proposed a method to generate cyclic gait patterns in [6] assuming no vertical acceleration of the CoG. In this paper, we extend it to consider the vertical acceleration of the CoG and the limit of the horizontal ground reaction force which changes according to the vertical acceleration.

Using these techniques, we can generate motions which satisfy the friction limit. Using the proposed methods, running at 10 km/h on a real robot whose leg dimension are the same as ASIMO (Fig. 1) is achieved.

Overview of motion generation and control system is given in section II, three different motion models for running is introduced in section III, synthesis of the motion models is explained in section IV, extension of cyclic walking gait generation techniques to running is given in section V, results in simulation and on real robot are given in section VI respectively.

Fundamental Research Center, Honda Research & Development, 8-1 Honcho, Wako-shi, Saitama, Japan.

II. System Overview

In this paper, a gait pattern is a set of trajectories for the desired ZMP, the feet and the upper body.

1. Given a command to move, step position and duration are decided (Fig. 2(a)).
2. Given parameters above, design the desired ZMP and feet trajectories. Then design the upper body trajectory which satisfies the desired ZMP trajectory without causing the upper body to diverge (Fig. 2(b)).
   2.1 Generate a gait pattern using a approximate dynamics model using estimate of the future model state (Fig. 2(d)).
   2.2 Compensate for the dynamics error due to the approximate dynamics model (Fig. 2(e)).
3. Command the gait pattern to the real robot, and stabilize it while it is following the gait pattern (Fig. 2(c)).

In this paper, gait pattern generation for running is discussed in detail. Basis for gait pattern generation for walking is explained in [6], the gait pattern modification to compensate approximated dynamics error is discussed in [7] and the integrated balance control is discussed in [8].

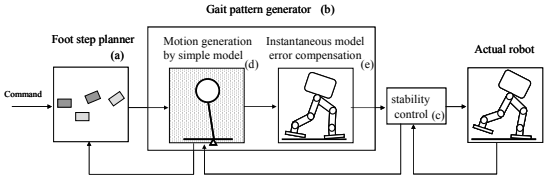

Fig. 2 System overview

III. Approximate Robot Dynamics Models

Running involves flight phases in which the ground reaction force becomes 0 and a physically feasible trajectory has to be in free fall motion. It is also required to keep the horizontal ground reaction force under limit during the support phases to prevent a slip. The limit of the horizontal ground reaction force is dependent on the vertical force and the friction coefficient. To better account for these requirements, we extend the three mass model in [6] with vertical and rotational motion models.

A. Vertical Motion

The vertical motion of the CoG of the robot is designed using the model from Fig. 3(a). This model has a point mass and its height varies as the robot moves vertically.

In [6] we proposed methods for generating cyclic gait patterns for walking. A cyclic gait consists of two steps, and the state of the vertical motion model has to be matched at the boundaries of a cyclic gait by definition.

Vertical acceleration of the CoG is designed as a series of straight line segments as shown in Fig. 4. The acceleration is $-g$ where g is the acceleration due to gravity during the flight phases and 0 during the double support phases. The vertical acceleration during the first step is shown in Fig. 4.

The vertical position and velocity of the CoG at the boundaries of a gait pattern has to be continuous by our definition of cyclic gaits.

Once the next cyclic gait is designed, the vertical trajectory of the CoG of the current gait pattern is modified to meet the boundary conditions at the end of the current gait pattern.

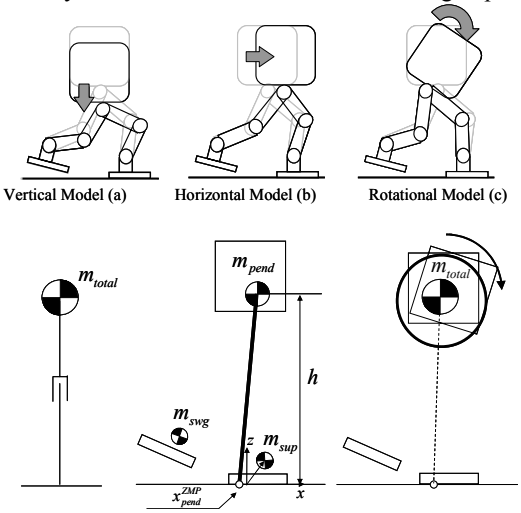

Fig. 3 Dynamics models

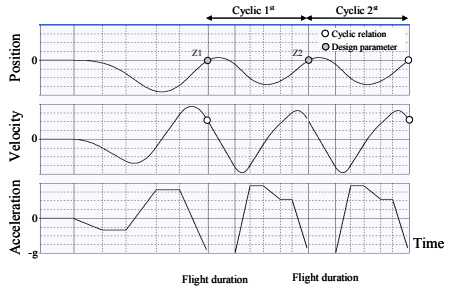

Fig. 4 Vertical motion

B. Horizontal Motion

Horizontal motion of the robot is designed using the model in Fig. 3(b). The model is similar to the one used in [6]. The height of the inverted pendulum changes due to the vertical motion, but it is assumed that the vertical motion from the vertical motion model is negligibly small compared to the natural height of the model and thus it is assumed to be a constant h.

m_{sup}, m_{swg} : The foot mass of the support and swing leg

m_{pend} : The mass of the inverted pendulum.

m_{total} : The total mass of the model ($= m_{pend} + m_{sup} + m_{swg}$).

x_{sup}, z_{sup} : The horizontal and vertical position of the foot of support leg.

x_{swg}, z_{swg} : The horizontal and vertical position of the foot of swing leg.

x_{pend} : The horizontal position of the inverted pendulum.

$\ddot{z}_{pend}$: The vertical acceleration of the inverted pendulum.

The ground reaction moment generated by the inverted pendulum about the origin is called the inverted pendulum moment M_{pend}.

$$M_{pend} = -m_{pend} x_{pend} (g + \ddot{z}_{pend}) + m_{pend} \ddot{x}_{pend} h \quad (1)$$

The acceleration of the inverted pendulum $\ddot{z}_{pend}$ is related to the vertical acceleration of the CoG as follows

$$m_{total} \ddot{z}_{cog} = m_{pend} \ddot{z}_{pend} + m_{sup} \ddot{z}_{sup} + m_{swg} \ddot{z}_{swg} \quad (2)$$

Arranging Eq. (1),

$$\ddot{x}_{pend} = \frac{(g + \ddot{z}_{pend})}{h} x_{pend} + \frac{1}{h \cdot m_{pend}} M_{pend} \quad (3)$$

The ground reaction moment about the origin due to the leg is called the leg moment M_{feet}.

$$\begin{aligned} M_{feet} = &-m_{sup} x_{sup} (g + \ddot{z}_{sup}) + m_{sup} \ddot{x}_{sup} z_{sup} \\ &- m_{swg} x_{swg} (g + \ddot{z}_{swg}) + m_{swg} \ddot{x}_{swg} z_{swg} \end{aligned} \quad (4)$$

C. Rotational Motion

The rotational motion about the CoG of the robot is approximated by the flywheel in Fig. 3(c).

I_{wheel}: The inertia matrix of the flywheel (only principal moments of inertia)

θ_{wheel} : The angle of the flywheel

M_{wheel} : The ground reaction moment due to the flywheel

The flywheel represents the motion of the robot in which moment is generated while the CoG stays still.

$$M_{wheel} = I_{wheel} \ddot{\theta}_{wheel} \quad (5)$$

Note that I_{wheel} is the characterized from the real robot. Inclining the upper body forward without translating it causes the CoG to move forward. To cancel it, the upper body has to be shifted horizontally by $C\theta_{wheel}$, where C is a constant. As implied in Eq. (5), the flywheel can generate a moment without generating ground reaction forces. The total moment due to the horizontal and rotational motions M_{total}.

$$M_{total} = M_{feet} + M_{pend} + M_{wheel} \quad (6)$$

We make use of these properties, and synthesize these two motions to generate the desired moment while satisfying the friction force limits.

IV. Synthesizing Motions with Friction Limit

The vertical motion of the robot is generated from the vertical motion model explained in section III-A. The limit of the horizontal ground reaction force F_{lim} is determined according to the friction coefficient of the ground and the vertical acceleration of the CoG. The shaded trapezoid regions in Fig. 5 are the range of horizontal force the biped robot can generate without causing a slip with the ground.

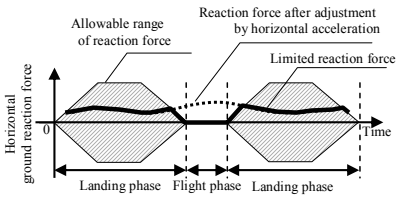

Fig. 5 Allowable range of horizontal reaction force

Given a command to run, feet trajectory and the desired total moment at each time step is generated. The total desired moment is the desired ZMP multiplied by the vertical ground reaction force. The desired ZMP trajectory is designed to go through the center of support polygon to have a large margin of stability. The desired ground reaction moment is 0 during the flight phases.

After obtaining M_{feet} from Eq. (4) and tentatively setting M_{wheel} to 0, M_{pend} can be computed from Eq. (6). Then $\ddot{x}_{pend}$ can be computed from Eq. (3) and it is integrated to obtain the velocity and the position of the inverted pendulum.

Now the total ground reaction force F_{total} is

$$F_{total} = m_{pend} \ddot{x}_{pend} + m_{sup} \ddot{x}_{sup} + m_{swg} \ddot{x}_{swg} \quad (7)$$

The value of F_{total} exceeding $[-F_{lim}, F_{lim}]$ cannot be achieved on the real robot (dashed line in Fig. 5), and thus the motion in Eq. (3) cannot be realized as it is. To fix this issue, the horizontal acceleration of the inverted pendulum model is limited to stay within the shaded regions. This also modifies the pendulum moment as follows.

$$M_{pend}^{mdfd} = \begin{cases} M_{pend} - h(F_{total} - F_{lim}) & (F_{total} > F_{lim}) \\ M_{pend} + h(F_{lim} + F_{total}) & (F_{total} < -F_{lim}) \\ M_{pend} & (else) \end{cases} \quad (8)$$

The flywheel, whose moment was tentatively set to 0, is used to compensate for the portion of M_{total} which the pendulum could not generate due to the ground reaction force limit.

$$M_{wheel} = M_{pend} - M_{pend}^{mdfd} \quad (9)$$

Substituting M_{pend}^{mdfd} into Eq. (3), modified value of $\ddot{x}_{pend}$ can be obtained, and $\ddot{\theta}_{wheel}$ can be obtained from Eq. (5). Integrating these, horizontal position and velocity of the inverted pendulum and the angle and angular velocity of the flywheel can be easily computed. With this modification, both the desired horizontal ground moment and the friction limits are satisfied.

V. Gait Pattern Generation

The horizontal and rotational motion models proposed in section IV can diverge as a result of generating required moments. Real robots have kinematic constraints and such motions cannot be realized. By meeting boundary conditions, divergence of the horizontal and rotational motions is prevented. This is achieved by proper design of the desired ZMP trajectory as explained in detail later. We proposed a similar approach to this problem for walking in [6], and it is

extended to running in this paper.

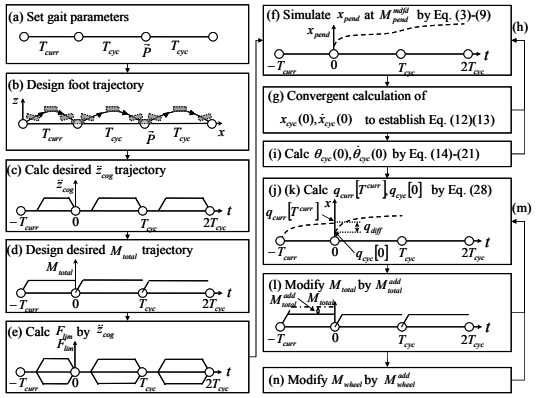

Fig. 6 Flow chart of gait generation with prediction

A. Flow of Gait Pattern Generation

Fig. 6 shows the processes involved in gait pattern generation. Given a command to move (a), the feet trajectory of the current and next cyclic gait patterns are computed (b). From them, the vertical motions of the current and next cyclic gait patterns are computed (c). The desired total moment trajectory is computed by multiplying the desired ZMP trajectory and vertical ground reaction force (d). The desired ZMP trajectory during single support phases are constructed from a series of straight lines. The friction force limits are determined from the vertical motion (e). In our system, a command to move consists of the step position and duration of the current gait and the first step of the next cyclic gait pattern.

The estimated states of the inverted pendulum and the flywheel models at the end of the next cyclic gait are computed as explained in section IV (f). By requiring the initial and terminal conditions of a cyclic gait pattern to match, the initial state of the inverted pendulum is computed iteratively (g)(h). The initial state of the flywheel is computed analytically, forcing the boundary conditions to match (i). The initial state of the inverted pendulum of a cyclic gait pattern is decomposed into the convergent and divergent components ([6]). The convergent component is ignored because it converges naturally over time, and thus the divergent component is used as the boundary condition (j).

Given the initial condition of the next cyclic gait pattern, the total moment trajectory of the current gait pattern is modified to meet it at the end of the current gait. The estimated states of the inverted pendulum and the flywheel models are computed at the end of the current gait (k). The total moment trajectory is modified (l) in such a way the divergent component at the end of the current gait matches with the initial condition of the next cyclic gait pattern (m). Finally, the flywheel moment of the current gait is modified to match the initial conditions of the next cyclic gait pattern (n).

The total desired moment is divided into the inverted pendulum and the flywheel models. From these, the position and angle of the upper body of the robot are determined. Solving inverse kinematics for them and feet trajectory, desired angle for each joint is computed and commanded to each joint.

B. Boundary Condition of the Inverted Pendulum Model of Cyclic Gait Pattern

For simplicity, we limit discussions about running motions for straight running in this paper. The following notations are used in this section.

T_{curr} : Period of the current gait

T_{cyc} : Period of the cyclic gait to be designed

$\vec{P}$:The ground contact position of the second support leg with respect to the ground contact position of the support leg of the current gait.

The coordinate frame whose origin is the second support leg is called the second coordinate frame (Fig. 7). Due to the design of the coordinate frame, the following is true.

$$x_{cyc}^{coord\,2}(T_{cyc}) = x_{cyc}(T_{cyc}) - \vec{P} \quad (10)$$

$$\dot{x}_{cyc}^{coord\,2}(T_{cyc}) = \dot{x}_{cyc}(T_{cyc}) \quad (11)$$

Also, the state of the robot at the end of current gait agrees with that at the beginning of the cyclic gait. Thus,

$$x_{cyc}^{coord\,2}(T_{cyc}) = x_{cyc}(0) \quad (12)$$

$$\dot{x}_{cyc}^{coord\,2}(T_{cyc}) = \dot{x}_{cyc}(0) \quad (13)$$

The initial velocity and position of the inverted pendulum satisfying Eq. (12)(13) are searched iteratively using the process shown in Fig. 6(f).

C. Boundary Condition of the Flywheel Model of Cyclic Gait Pattern

As explained in section IV, the flywheel model rotates to generate moments. Similar to the inverted pendulum model, the flywheel model is also required to have same initial and terminal states for a cyclic gait pattern. The following notations are used in this section.

$\theta_{cyc}(t)$: The angle of the flywheel at time t

$\dot{\theta}_{cyc}(t)$: The angular velocity of the flywheel at time t

$\theta_{sim}(T_{cyc})$, $\dot{\theta}_{sim}(T_{cyc})$: The angle and angular velocity of the flywheel at the end of the cyclic gait pattern due to M_{wheel} in Eq. (8)(9)

Note that t is 0 at the beginning of the cyclic gait pattern. Due to the design of the coordinate frame,

$$\theta_{cyc}^{coord\,2}(T_{cyc}) = \theta_{cyc}(T_{cyc}) \quad (14)$$

$$\dot{\theta}_{cyc}^{coord\,2}(T_{cyc}) = \dot{\theta}_{cyc}(T_{cyc}) \quad (15)$$

Because of the cyclic properties, the followings are true.

$$\theta_{cyc}^{coord\,2}(T_{cyc}) = \theta_{cyc}(0) \quad (16)$$

$$\dot{\theta}_{cyc}^{coord\,2}(T_{cyc}) = \dot{\theta}_{cyc}(0) \quad (17)$$

A moment in the shape of a trapezoid of height K_{wheel} (Fig. 8), $M_{wheel}^{add}(t)$, is added so that the boundary conditions of the flywheel match to satisfy the cyclicity requirement. $M_{wheel}^{add}(t)$ can be transformed into the angle and angular velocity at the

end of the gait pattern, C_θ and C_ω using Eq. (5).

$$\theta_{add}(T_{cyc}) = K_{wheel} C_\theta \quad (18)$$

$$\dot{\theta}_{add}(T_{cyc}) = K_{wheel} C_\omega \quad (19)$$

The followings are true about the dynamics of the flywheel.

$$\theta_{cyc}(T_{cyc}) = \theta_{cyc}(0) + \dot{\theta}_{cyc}(0) T_{cyc} + \theta_{sim}(T_{cyc}) + \theta_{add}(T_{cyc}) \quad (20)$$

$$\dot{\theta}_{cyc}(T_{cyc}) = \dot{\theta}_{cyc}(0) + \dot{\theta}_{sim}(T_{cyc}) + \dot{\theta}_{add}(T_{cyc}) \quad (21)$$

Setting the angle at the beginning of the second step to 0 and solving Eq. (14)-(21), the values of $\dot{\theta}_{cyc}(0)$ and K_{wheel} are computed.

M_{wheel} and M_{total} must be modified by the same amount to not modify the behavior of the inverted pendulum model. On the other hand, M_{total} is computed from the desired ZMP trajectory to have large region of stability and major modification to it is undesirable.

To reconcile this issue, the following two stage scheme is employed. In the first iteration, M_{wheel} is computed while fixing M_{total}, then the initial state of the inverted pendulum is recomputed. In the second iteration, M_{total} is modified hoping it is minor.

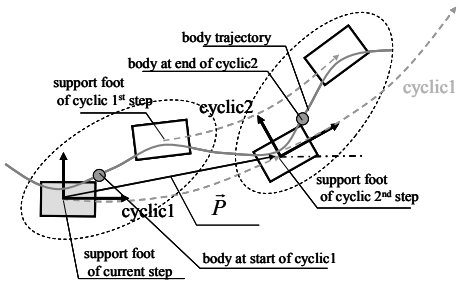

Fig. 7 Coordinate system of cyclic gait pattern

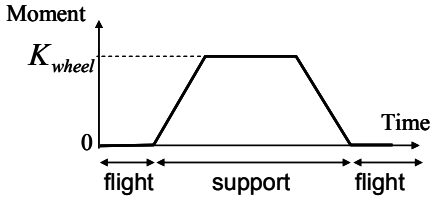

Fig. 8 Wheel moment

D. Divergent Component with Vertical Acceleration

We proposed a notion of convergent and divergent components for walking[6], and used the divergent component as relaxed boundary condition between the current and next cyclic gait patterns. The convergent component converges over time without being controlled and the divergent component diverges. From these properties, only the divergent component needs be considered when generating gait patterns.

Due to the vertical motion, the divergent component of running is different from that of walking. We define the divergent and convergent components for running as follows. Rewriting Eq. (3) into state equation form in continuous time, $\dot{\mathbf{x}} = A(t)\mathbf{x} + B(t)\mathbf{u}$, $\mathbf{x} = \begin{pmatrix} x & \dot{x} \end{pmatrix}^T$ and $\mathbf{u} = M_{pend}$ where

$$A(t) = \begin{pmatrix} 0 & 1 \\ \dfrac{(g + \ddot{z}_{pend})}{h} & 0 \end{pmatrix}, B(t) = \frac{1}{h \cdot m_{pend}} \quad (22)$$

In discrete time,

$$\mathbf{x}_{k+1} = A(k)\mathbf{x}_k + B(k)\mathbf{u}_k \quad (23)$$

where ΔT is the time step of this discrete system.

For $g + \ddot{z}_{pend} > 0$

$$A(k) = \begin{pmatrix} \dfrac{e^{\omega_0 \Delta T} + e^{-\omega_0 \Delta T}}{2} & \dfrac{e^{\omega_0 \Delta T} - e^{-\omega_0 \Delta T}}{2\omega_0} \\ \dfrac{e^{\omega_0 \Delta T} - e^{-\omega_0 \Delta T}}{2} \omega_0 & \dfrac{e^{\omega_0 \Delta T} + e^{-\omega_0 \Delta T}}{2} \end{pmatrix},$$

$$B(k) = \frac{1}{\omega_0^{\,2} \cdot h \cdot m_{pend}} \begin{pmatrix} 1 - \dfrac{e^{\omega_0 \Delta T} + e^{-\omega_0 \Delta T}}{2} \\ -\dfrac{e^{\omega_0 \Delta T} - e^{-\omega_0 \Delta T}}{2} \omega_0 \end{pmatrix}$$

For $g + \ddot{z}_{pend} = 0$,

$$A(k) = \begin{pmatrix} 1 & \Delta T \\ 0 & 1 \end{pmatrix}, B(k) = \begin{pmatrix} \dfrac{(\Delta T)^2}{2} \dfrac{1}{h \cdot m_{pend}} \\ \Delta T \dfrac{1}{h \cdot m_{pend}} \end{pmatrix}$$

For $g + \ddot{z}_{pend} < 0$,

$$A(k) = \begin{pmatrix} \cos(\omega_0 \Delta T) & \dfrac{\sin(\omega_0 \Delta T)}{\omega_0} \\ -\sin(\omega_0 \Delta T)\omega_0 & \cos(\omega_0 \Delta T) \end{pmatrix},$$

$$B(k) = \begin{pmatrix} \dfrac{1}{\omega_0^{\,2} \cdot h \cdot m_{pend}} \cdot \left(\cos(\omega_0 \Delta T) - 1\right) \\ -\dfrac{1}{\omega_0 \cdot h \cdot m_{pend}} \cdot \sin(\omega_0 \Delta T)\omega_0 \end{pmatrix}$$

where $\omega_0 = \sqrt{\left| g + \ddot{z}_{pend} \right| / h}$. State transition matrices are time dependent due to $g + \ddot{z}_{pend}$. Note that $g + \ddot{z}_{pend}$ can become negative if the legs are accelerated upwards during the flight phases as implied in Eq. (2).

Given initial state $\mathbf{x}_0$, Eq. (23) becomes

$$\mathbf{x}_k = \phi(k,0)\mathbf{x}_0 + \sum_{l=0}^{k-1} \phi(k, l+1) B(l) \mathbf{u}_l \quad (24)$$

$$\phi(k,0) = A(k-1)A(k-2)\cdots A(0) \quad k > 0 \quad (25)$$

Let $\mathbf{x}_{cyc}(0)$ be the initial state of the cyclic gait pattern and be the duration of the cyclic gait pattern as a number of time steps, then,

$$\mathbf{x}_{cyc}(k_{cyc}) = \phi(k_{cyc}, 0)\mathbf{x}_{cyc}(0) \quad (26)$$

Let transfer function Γ_{cyc} formed by the columns of the eigenvectors of $\phi(k_{cyc}, 0)$, and $\Lambda = \Gamma_{cyc}^{-1} \phi(k^{cyc}, 0) \Gamma_{cyc}$ be the diagonalized matrix of $\phi(k_{cyc}, 0)$,

$$\Gamma_{cyc}^{-1} \mathbf{x}_{cyc}(k_{cyc}) = \Lambda \Gamma_{cyc}^{-1} \mathbf{x}_{cyc}(0) \quad (27)$$

Now we define the convergent and divergent component at the beginning of the cyclic gait pattern, p and q respectively,

for running as follows.

$$\begin{pmatrix} p \\ q \end{pmatrix} = \Gamma_{cyc}^{-1}\mathbf{x} \tag{28}$$

The system diverges if $\lambda > 1$ and converges otherwise. It is designed such that p corresponds to λ_1 and q corresponds to λ_2. We assume $\lambda_1 < 1, \lambda_2 > 1$ for running in which the support and flight phases are repeated. The friction limit is not considered in the definition of the convergent and divergent components. Using Eq. (28), the initial state of the inverted pendulum is transformed into the initial divergent and convergent components.

E. Satisfying Boundary Condition for the Inverted Pendulum

The modification to the current ZMP trajectory tends to be small when using the divergent component as the required boundary condition instead of position and velocity [6]. From the leg trajectories and the desired ZMP trajectory, the expected states of the inverted pendulum and the flywheel at the end of the current gait are computed with Eq. (8)(9). These are transformed into $q_{curr}(T_{curr})$ using Eq. (28), and the difference q_{diff} from the divergent component at the beginning of the next cyclic gait is

$$q_{diff} = q_{cyc}(0) - q_{curr}(T_{curr}) \tag{29}$$

M_{total}^{add} is the modification to M_{total} given in the shape of a trapezoid(Fig. 9). The height of the trapezoid which makes Eq. (29) 0 can be computed iteratively.

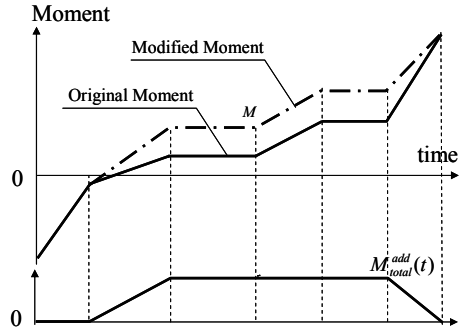

Fig. 9 Total moment modification

F. Satisfying Boundary Condition for the Flywheel

The difference between the expected state of the flywheel at the end of current gait and the initial state at the beginning of the next cyclic gait pattern is easily computed. The effect M_{wheel} has over the angle and angular velocity of the flywheel can be computed from Eq. (5). Choosing proper height of the M_{wheel} trajectory shown in Fig. 8, the error can be canceled to 0.

On the real robot, M_{wheel} is modified over the current step and the first step of the next cyclic gait pattern to avoid rapid change of the originally designed trajectory.

VI. RESULTS

A. Divergent Component with Vertical Acceleration

The definitions of the divergent component with and without vertical acceleration term are compared (Fig. 10). The divergent component of a cyclic gait for running at 5.1 km/h is computed from two different equations. Line(a) in Fig. 10 shows the trajectory generated using the divergent component computed from Eq. (28), and Line(b) shows the trajectory generated using the divergent component computed from Eq. (11) of [6]. It is observed that using the previously proposed definition of the divergent component, the inverted pendulum stays behind the desired angle and the boundary condition is not met. With the newly proposed definition, current trajectory connects to the next cyclic gait pattern successfully.

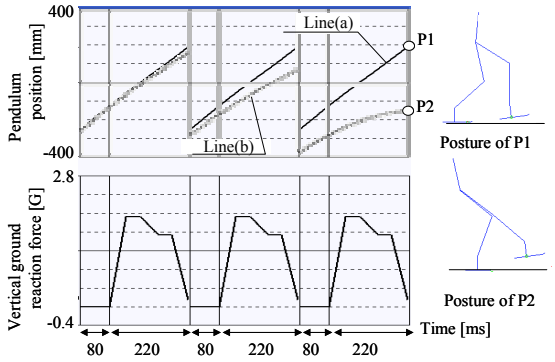

Fig. 10 Comparison of two divergent components

B. Gait Pattern Generation

Using a robot with the same dimension of legs as ASIMO, a gait pattern for running at 6 km/h was generated on simulation. Switch was made over three steps to avoid too large modification to the moment. The first step, the step being taken when the switch is commanded, originally had the step length of 400 mm and duration of 315 ms (flight phase is 80 ms long and support phase is 235 ms). The first step is modified to the step length of 525 mm and duration of 315 ms. The second step has length of 525 mm and duration of 315 ms.

Fig. 11 shows, from the top, the desired vertical ground reaction force and the vertical acceleration of the inverted pendulum $(g + \ddot{z}_{pend})$, M_{total} before and after modification, the horizontal position of the inverted pendulum, the angle of the flywheel, the angular acceleration of the flywheel, the actual horizontal ground reaction force and its limit.

It can be observed that the vertical acceleration of the inverted pendulum becomes negative during the flight phase due to the motion of the feet mass. The horizontal ground reaction force stays within the limit. The flywheel accelerates to generate the required moment around the flight phases where available ground reaction force is small, and it accelerates in the other direction to prevent diverging during the support phases.

The flywheel does not follow a cyclic trajectory because the boundary condition for the inverted pendulum is the divergent component and the horizontal ground reaction force differs from the expected value. However this could be solved by using position and velocity as the boundary conditions for the inverted pendulum, this is a minor effect and can be ignored in reality.

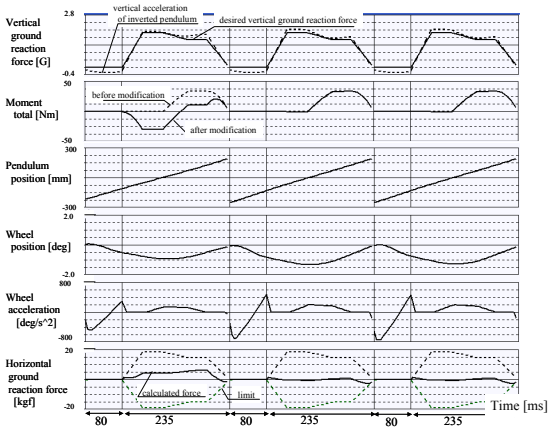

Fig. 11 Trajectories of inverted pendulum and flywheel model for running at 6 km/h

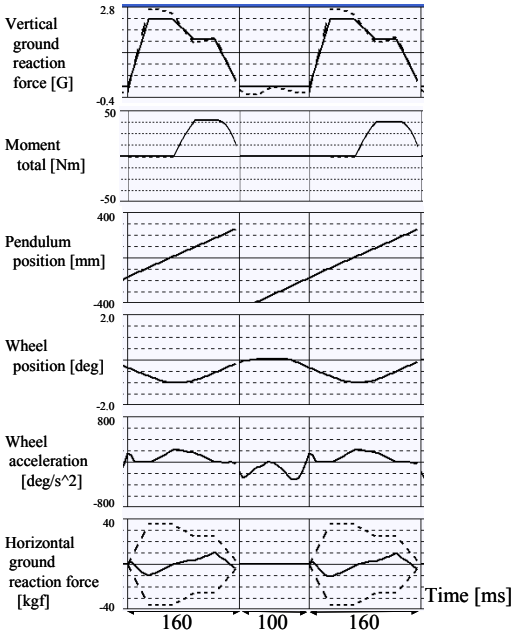

Fig. 12 Trajectories of inverted pendulum and flywheel model for running at 10 km/h

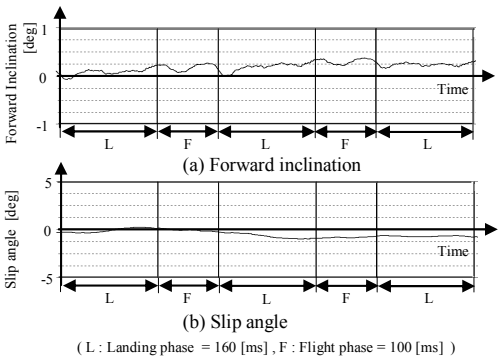

Fig. 13 Upper body trajectory for running at 10 km/h

C. Running Experiment on a Real Robot

On a real robot whose leg dimension are the same as that of ASIMO with lighter weight and more powerful actuators, running at 10 km/h was achieved. The desired trajectory of this 10 km/h running is shown in Fig. 12. On the real robot, the upper body of the robot rotates about the vertical axis to prevent falling sideways. This motion is independent from other axes and relatively easily implemented. The trajectory is compensated for dynamics model error as explained in [7] before it is fed to the robot, and it is controlled as explained in [8].

Fig. 13(a) is the inclination error of the upper body in the sagittal plane, and Fig. 13(b) is the rotation of the upper body about the axis vertical to ground. The upper body angle is estimated from a gyro sensor and an accelerometer. The upper body angle stays within ± 0.4 deg and the spin stays $\pm$ 1.0 deg.

VII. CONCLUSIONS

We proposed decomposition of running motion for biped robots into vertical, horizontal and rotational components. Using this technique, generation of robust gait in which the horizontal ground reaction force stays within the limit for motions in which the ground friction force becomes small around the flight phases. These techniques can be easily applied to intermediate motions between walking and running involving no flight phase or walking on ground with small friction coefficients.

We also proposed an extension to the divergent component to take the vertical acceleration of the CoG into account for running. The effectiveness of the proposed extension was shown in simulation.

Combining these techniques, we achieved running at 10 km/h on a robot who has same dimension as ASIMO.

REFERENCES

[1] K. Hirai, M. Hirose, Y. Haikawa, and T. Takenaka, "The Development of Honda Humanoid Robot", In Proceedings of the 1998 IEEE International Conference on Robotics and Automation, Leuven, Belgium, May. 1998, pp. 1321-1326.

[2] Y. Sakagami, R. Watanabe, C. Aoyama, S. Matsunaga, N. Higaki, and K. Fujimura, "The intelligent ASIMO: System overview and

integration", In Proceedings of the 2002 IEEE/RSJ International Conference on Intelligent Robots and Systems, 2002, pp. 2478-2483.
[3] T. Nagasaki, S. Kajita, K. Kaneko, K. Yokoi, K. Tanie, "A Running Experiment of Humanoid Biped", In Proceedings of 2004 IEEE/RSJ International Conference on Intelligent Robots and Systems, 2004, pp. 136-141.
[4] K. Nagasaka, Y. Kuroki, S. Suzuki, Y. Itoh, and J. Yamaguchi, "Integrated Motion Control for Walking, Jumping and Running on a Small Bipedal Entertainment Robot", In Proceedings of the 2004 IEEE International Conference on Robotics and Automation, New Orleans, 2004, pp. 3189-3194.
[5] R.Tajima, D.Honda and K.Suga, "Fast Running Experiments Involving a Humanoid Robot", IEEE International Conference on Robotics and Automation, 2008, pp. 1571-1576
[6] T. Takenaka, T. Matsumoto, and T. Yoshiike, "Real Time Motion Generation and Control for Biped Robot –1st Report: Walking Gait Pattern Generation-", In Proceedings of IEEE/RSJ International Conference on Intelligent Robots and Systems, 2009.
[7] T. Takenaka, T. Matsumoto, and T. Yoshiike, "Real Time Motion Generation and Control for Biped Robot -3rd Report: Gait Pattern Modification to Compensate Approximated Dynamics Error-", In Proceedings of IEEE/RSJ International Conference on Intelligent Robots and Systems, 2009.
[8] T. Takenaka, T. Matsumoto, T. Yoshiike, T. Hasegawa, S. Shirokura, H. Kaneko, and A. Orita, "Real Time Motion Generation and Control for Biped Robot -4th Report: Integrated Balance Control-", In Proceedings of IEEE/RSJ International Conference on Intelligent Robots and Systems, 2009.
[9] S. Kajita, O. Matsumoto, and M. Saigo, "Real-time 3D Walking Pattern Generation for a Biped Robot with Telescopic Legs", In Proceedings of the 2001 IEEE International Conference on Robotics and Automation, 2001, pp. 2299-2306.
[10] Y.Fujimoto, "Trajectory Generation of Bipedal Running Robot with Minimum Energy Consumption", In Proceedings of IEEE International Conference on Robots and Automation, 2004, pp. 3803-3808.
[11] T.Sugihara and Y.Nakamura, "Enhancement of Boundary Condition Relaxation Method for 3D Hopping Motion Planning of Biped Robots", In Proceedings of the 2007 IEEE/RSJ International Conference on Intelligent Robotics and Systems, San Diego, 2007, pp. 444-449.
[12] M.H.Raibert, Legged Robot that Balance, MIT Press, 1986.
[13] O. Kwon and J.H.Park, "Gait Transitions for Walking and Running of Biped Robots", In Proceedings of the 2003 IEEE International Conference on Robotics and Automation, Taipei, Taiwan, September, 2003, pp. 1350-1355.
[14] J.Pratte, J.Carff, S.Drakunov and Ambarish Goswami, "Capture Point: A Step toward Humanoid Push Recovery", In Proceedings of the 2006 IEEE International Conference on Humanoids, 2006, pp. 200-207.